Systematic analysis of symmetry energy effects in the neutron star crust properties

S.Kubis and D.E. Alvarez-Castillo
H.Niewodniczański Institute of Nuclear Physics, Radzikowskiego 152, 31-342 Kraków, Poland

The functional form of the nuclear symmetry energy in the whole range of densities relevant for the neutron stars is still unknown. Discrepancies concern both the low as well as the high density behaviour of this function. By use of Bézier curves three different families of the symmetry energy shapes, relevant for different density range were introduced. Their consequences for the crustal properties of neutron stars are presented.

I. INTRODUCTION

The basic quantity in the description of infinite nuclear matter filling out the interior of neutron star is the energy per particle expressed in term of baryon number density $n = n_p + n_n$ and isospin asymmetry $\alpha = \frac{n_n - n_p}{n}$ of the system:

$$E(n,\alpha) = V(n) + E_s(n)\,\alpha^2 + \mathcal{O}(\alpha^4) \tag{1}$$

Instead of α it is useful to use proton fraction x, and then $\alpha = (1-2x)$. Here we assumed the only constituents of stellar matter are nucleons and leptons: electrons and muons. Around and above the nuclear density $n_0 = 0.16$ fm^{-3} nucleons and leptons form a quantum liquid, which stands for liquid core of the neutron star. Slightly below n_0 matter cannot exist as a homogeneous fluid - the one-phase system is unstable and the coexistence of two phases is required. At these densities matter clusterizes into positive nuclei immersed in a quasi-free gas of neutrons and electrons. Model calculations show this type of matter forms a Coulomb lattice with solid state properties and corresponds to the crust covering liquid core of a star. The presence of the crust is affirmed by the glitching phenomenon observed for some pulsars. For typical NS masses, between 1-2 $M_\odot$, the most of the stellar matter is occupied by the core, so the global parameters like the mass, radius, moment of inertia are completely determined by the functional form of the Eq. (1). Whereas the isoscalar part $V(n)$ corresponds mainly for the stiffness of Equation of State (EOS) which is relevant for the maximum mass of NS, the isovector part $E_s(n)$ is responsible for the chemical composition of the matter. Through the β-equilibrium equations

$$4(1-2x)E_s(n) = \mu_n - \mu_p = \mu_e = \mu_\mu \tag{2}$$

the proportions of all particles are determined. The symmetry energy is also relevant for the crust-core transition in NS as it was shown in [1]. It's role can be explicitly seen if one looks at the compressibility under constant chemical potential relevant for the stability of homogeneous beta equilibrated nuclear matter:

$$K_\mu = n^2(E_s''\alpha^2 + V'') + 2n(E_s'\alpha^2 + V') - \frac{2\alpha^2 E_s'^2 n^2}{E_s}, \tag{3}$$

and when $K_\mu > 0$ the matter is stable. This formula accounts for the bulk approximation and can be improved by inclusion of finite size effects like Coulomb and surface contributions. Such corrections were studied in [4] were it was shown that

$$v(Q) = v_{min} = v_0 + 2(4\pi e^2\beta)^{1/2} - \beta k_{TF}^2 \tag{4}$$

is the minimal value for stable density modulations for the Q momentum. Stability of matter is given by the condition $v(Q) > 0$. Note that the vanishing of v_0 is equivalent to the vanishing of K_μ since they are related by

$$v_0(n) = \frac{8K_\mu(n)E_s(n)}{n^2}\left(\frac{\partial\mu_n}{\partial n_n}\right)^{-1}. \tag{5}$$

Both of these approaches consider stability of a one phase system against density fluctuations. However there exists another approach based on treating the NS crust as a two component system subject to the Gibbs conditions for mechanical and chemical stability expressed by:

$$p^I = p^{II} \quad , \quad \mu_n^I = \mu_n^{II} \quad , \quad \mu_e^I = \mu_e^{II}. \tag{6}$$

Where the first component (I) corresponds to clusters composed of protons and neutrons immersed in a pure neutron liquid (II) component. Both phases are permeated by degenerated electrons. As density increases towards the star interior the two phase system can no longer exist and it signals the crust-core transition. These approaches correspond to three different critical densities $n_c(K_\mu)$, $n_c(Q)$, and $n_c(1 \leftrightarrow 2)$ which will be presented for various models in the following sections.

In this work we are interested in the crustal properties, so it seems natural to focus on the symmetry energy form around saturation density n_0, to which the critical density n_c is closely located. However, as was suggested in [2] the crust is affected by the star compactness which depends on the E_s form at densities much higher than n_0. Furthermore recent experimental measurements [3] show non-standard behaviour of E_s at densities much below n_0. All these issues lead us to the idea to somehow "factorize" the shape of E_s to see how symmetry energy at different ranges of density affects the NS crust. It appeared to be possible to define models in which the E_s is changing at chosen range of density whereas the rest of its shape is kept the same. We have constructed the three main families of models with varying shape at very low, $n \to 0$, intermediate $n \approx n_0$ and very high densities $n \gg n_0$. The work is organized as follows: in the

section II we present recent experimental data useful in constraining the form of the symmetry energy, in the section III the construction of different models is shown. In the last two sections the results of the calculation and the astrophysical constraints coming form NS observations are discussed.

II. MEASURED SYMMETRY ENERGY PROPERTIES IN LABORATORY EXPERIMENTS

The symmetry energy E_s properties around saturation density can be inferred from laboratory experiments. For nuclei, it corresponds to the volumetric symmetry energy term S_v in the liquid droplet model [5]: $E_s(n_0) = S_v$, which also contains the surface contribution to the symmetry energy S_s. By measuring in nuclei these two quantities is possible to derive $E_s(n_0)$ and L which is related to its slope

$$L = 3n_0 \frac{\partial E_s(n)}{\partial n}\bigg|_{n_0}. \tag{7}$$

Not precisely available at the moment from experiments but also relevant for NS matter is the curvature of the symmetry energy:

$$K_s = 9n_0^2 \frac{\partial^2 E_s(n)}{\partial n^2}\bigg|_{n_0}. \tag{8}$$

Neutron rich nuclei feature halos composed mainly of neutrons while most of the protons stay in nuclear cores. Such neutron skin thickness is dependent on both volumetric and surface symmetry energies (by means of the coefficient S_v/S_s) and provides another way of measuring $E_s(n_0)$. S_v itself can be extracted from heavy ion collisions where isospin diffusion occurs: two colliding nuclei with opposite neutron abundances exchange components reaching isospin equilibration. Both, neutron skin thickness measurements [6] and isospin diffusion [7] shows that L is placed in the range between 40 and 80 MeV.

Experiments allows for measurements of asymmetric matter compressibility K_{asy} being related to K_s by the approximate relation $K_s \approx K_{asy} + 6L$. Recent experimental analysis [8–10] shows that K_{asy} takes values between -650 and -400 MeV. It means that, including the discrepancies of L, one may estimate that K_s is in a broad range between -400 and 100 MeV.

The density around n_0 is the natural place where the efforts in determining of symmetry energy behavior are focused. However even if the values of slope L or the curvature K_s achieve satisfactory accuracy the symmetry energy shape remains uncertain in both very low and very high density which are relevant for NS properties. For some years, the very low density part of the nuclear energy has been studied as well [3, 11]. In these works the symmetry energy is probed at $n \approx 10^{-2}$ fm^{-3} and appears to take large values ~ 10 MeV at this range of density. The result is very interesting. First, it allows for going beyond the poor and not very restrictive expansion around the n_0, and secondly it is highly relevant for the crust-core transition in neutron star.

III. BÉZIER CURVES FOR THE SYMMETRY ENERGY

For a good description of the neutron star properties it is important to know the symmetry energy functional form in the whole range of densities. From the aforementioned measurements one can pin down the symmetry energy properties around saturation but both low and high density parts are not well determined. Therefore there is large freedom to assume the behavior of $E_s(n)$ and introduce different parametrization.

Previously used parametrization (often polynomials) were not convenient since once the same saturation point properties are fulfilled the values far from saturation are fixed, thus sometimes leading to unphysical results, like unstable EOS (MDI parametrization) for large negative vales of E_s at high densities [2]. Polynomial interpolation presents some advantages as it may produce any shape but might present problems when derivatives are computed. At the boundary of the domains of interpolation the analicity is lost. In particular for pressure and compressibility the first and second derivatives are required and such polynomial interpolation leads to artifacts in the EOS. On the contrary Bézier curves [12] allow for

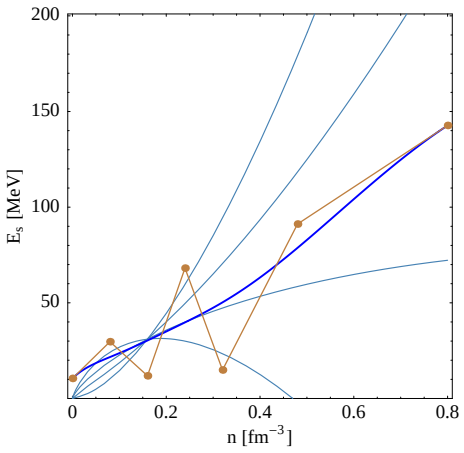

FIG. 1. Bézier Curve (thick blue) for seven control points (brown). The thin lines represent symmetry energies for the MDI models shown as a reference.

construction of different E_s shapes that respect saturation properties, like $E_s(n_0)$ and L, but can take any value at low and high density values, see Fig. 1. The resulting Bézier curve is then an analytical function that offers big advantages over interpolated functions.

Bézier curve of degree n is based on $n+1$ control points $\mathbf{P}_i$, where $i = 0, 1, 2 \ldots n$. For implementation purposes,

an arbitrary number of control points can be chosen to cast the curve shape as desired by means of the following relation:

$$\mathbf{B}(t) = \sum_{i=0}^{n} \binom{n}{i} (1-t)^{n-i} t^i \mathbf{P}_i, \qquad t \in [0,1] \qquad (9)$$

where $\binom{n}{i}$ is the binomial coefficient.

The constructed models for E_s are presented in the following subsections and their control points are tabelarized in the appendix. As we are interested only in the symmetry energy effects, the isoscalar part $V(n)$ in the Eq.(1), required for the of the full nuclear model, is kept all the time the same. We used the functional form taken from [13] for which the symmetric matter compressibility is $K_0 = 240$ MeV.

A. Low density symmetry energy effects and the neutron clusterization problem

In an earlier work the authors implemented a set of models motivated by the low density behaviour of the symmetry energy that were introduced to explore NS properties [2]. However a detailed analysis of phase transitions revealed pathological properties. Fig. 2 shows the phase diagram of a model similar to the earlier $k10$ in which $E_s(n \sim 0) = 10$ MeV and for which the thermodynamical Gibbs conditions hold. In it, the region to the left of the spinodal line (in red) where the proton fraction is zero (pure neutron matter) is reached by isobaric lines of negative pressure which indicates clusterization of neutrons. This is in disagreement with common knowledge that neutrons never clusterize. Here we propose a method avoiding this pathology. In order to keep finite values of E_s at vanishing density it is then necessary to

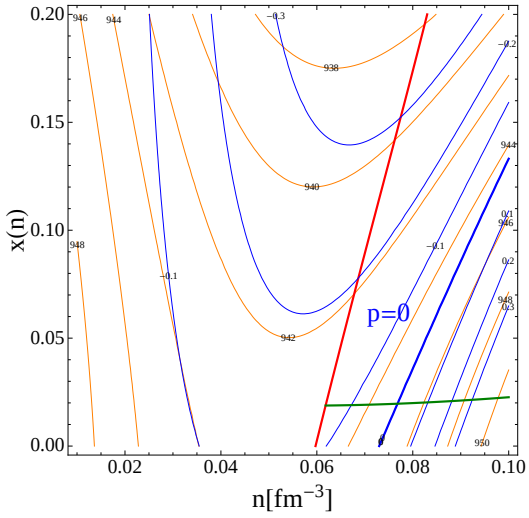

FIG. 2. $\Delta E - k10$ model in which $E_s(0) = 10$ MeV. Clusterization of pure neutron matter occurs when the energy per baryon is given by $\tilde{E}(n,x)$.

correct the whole expression for the total energy of nuclear matter. First, we introduce the following symmetry energy expression:

$$E_s(n) = \begin{cases} E_s^{PALu}(n) + E_s^{Bézier,k}(n) & \text{if } n < n_0 \\ E_s^{PALu}(n) & \text{if } n > n_0, \end{cases}$$

where $E_s^{PALu}(n)$ is the symmetry energy introduced in the work [13] with the interaction part $F(u) = u$. $E_s^{Bézier,k}(n)$ is a Bézier curve that modifies the low density part in such a way that $E_s^{Bézier,k}(0) + E_s^{PALu}(0) = k$, k being any value in MeV. In this way, $E_s(n)$ can take the $k = E_s(0)$ value for which the corresponding Bézier curve is designed for. With it, the energy per particle becomes:

$$\tilde{E}(n,x) = V(n) + (1-2x)^2 E_s(n). \qquad (10)$$

The above formula still needs to be corrected for neutron clusterization. In order to *avoid neutron clusterization*, the following correction is defined:

$$\Delta E(n) = \begin{cases} E_s^{Bézier}(n) & \text{if } n < n_0 \\ 0 & \text{if } n > n_0, \end{cases}$$

so that the final form of the energy is given by

$$E(n,x) = \tilde{E}(n,x) - \Delta E(n). \qquad (11)$$

We call ΔE-k models when the above modifications are applied. In fact, the symmetry energy can be recovered by definition:

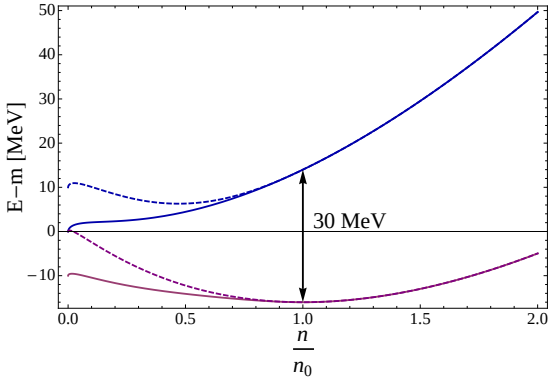

FIG. 3. Energy per particle $E(n,x)$ for the ΔE-$k10$ model with correction (solid lines) and without it: $\tilde{E}(n,x)$(dashed lines). The blue lines correspond to pure neutron matter while the purple ones correspond to symmetric nuclear matter.

$$E_s(n) = E(n, x=0) - E(n, x=\frac{1}{2}). \qquad (12)$$

and captures the features of the k models (finite symmetry energy values at almost zero baryon density). At saturation point these models have the same values as the PALu model (in MeV):

$$E_s(n_0) = 30, \qquad L = 77, \qquad K_s = -26.$$

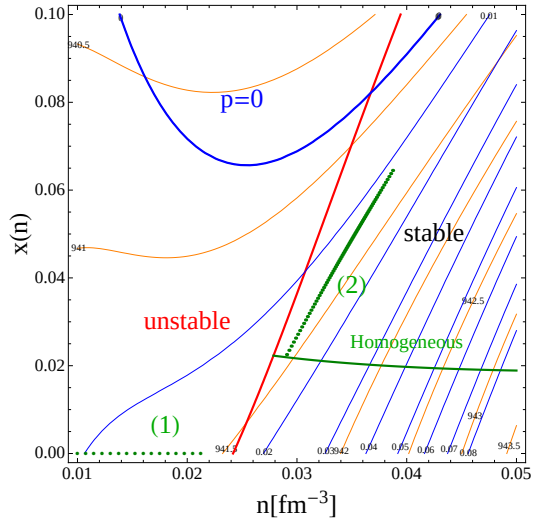

FIG. 4. ΔE-*k10* model in which $E_s(0) = 10$ MeV. Clusterization of pure neutron matter is now impossible for this model when the ΔE correction is included. Close to the spinodal (in red), the system splits into two phases, (1) - pure neutron (2) - nuclear matter represented by dotted green lines.

Let us recall that the $E_s^{Bézier}$ curves where defined in such a way to preserve the known properties of symmetric nuclear matter, i.e., its compressibility at saturation and its minimum. These conditions are fulfilled because the following derivatives with respect to baryon number density vanish at saturation:

$$\begin{aligned} \Delta E'(n_0) &= 0, \\ \Delta E''(n_0) &= 0. \end{aligned} \tag{13}$$

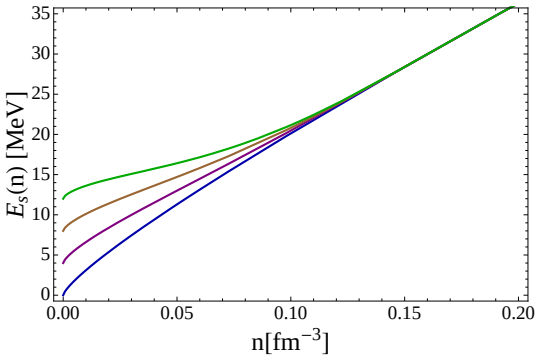

FIG. 5. Nuclear symmetry energy for ΔE-k models. The curves correspond to $E_s(0) = 0, 4, 8, 12$ MeV.

B. Different symmetry energy slopes at saturation density

The importance of the slope of the symmetry energy for the NS crust-core transition point can be easily seen in Eq. (3). The last term in that equation is the one responsible for the stability breaking and includes the square of the symmetry energy slope. The measured value of L will influence the behaviour of E_s away from saturation. In this section we introduce two families of models with the same symmetry energy forms at high and low densities but with variable slope at saturation point. There at saturation, they share the common values

$$E_s(n_0) = 31, \qquad K_s = 0.$$

whereas the slope L takes values in the range between 40-120 MeV corresponding to those reported by various experiments [21]. These properties are established by joining two Bézier curves describing the low and high density parts joint at saturation point with continuous derivatives up to second order. At low densities all of them go to zero while at high densities they follow the behavior of either b or c MDI models [2]. The two families are presented in Fig. 6. The reason of introducing the b or c-like behaviour at high densities comes from the analysis of direct URCA constraint which is discussed in detail in the subsection D.

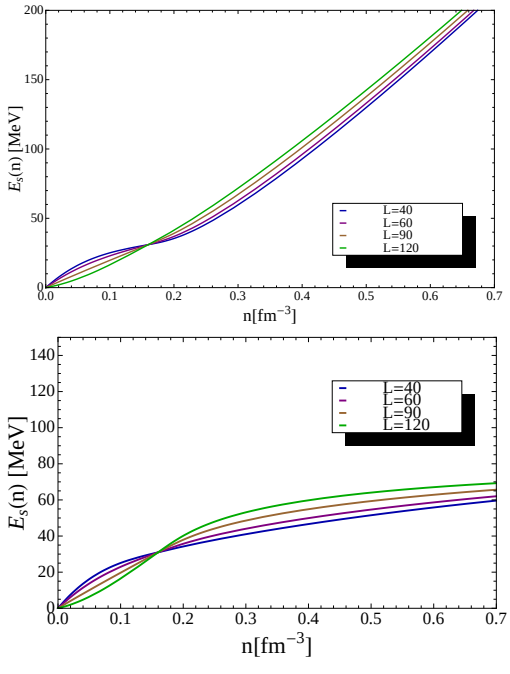

FIG. 6. Different symmetry energy shapes for the *L-high-c* models (top) and for *L-high-b* (bottom).

C. High density region symmetry energy effects

The critical density for the crust-core transition is the most relevant quantity for determination of the NS crust properties. Its value determines the crust thickness and moment of inertia. The crust-core position depends only on the behavior of the symmetry energy below saturation. However the crust thickness is not only determined by the critical density but also by the global parameters of the NS like its mass and radius. Those global parameters depend on the high density part of E_s. To explore such effects we construct a set of models with the same low density part implying the same crust-core transition but with different high density part. In relation to that, the authors of [14] derive an approximate formula assuming a polytropic equation of state for a thin, light crust but deviations from those assumptions can lead to completely different results and are due to the high density E_s region, as will be presented in the following sections. We introduce the *high-*E_s models which have the following values (in MeV):

$$E_s(n_0) = 31, \qquad L = 60, \qquad K_s = 0$$

and are composed of two Bézier curves describing both the low and high density parts joint at saturation point with continuous derivatives, just like in the previous models for variable slopes. They are named b, c, d since they possess the same high density values as the corresponding b, c, d MDI models [2]. The e model is an extreme case whose values grow much faster with increasing density than the rest. Fig. 7 shows E_s for all of them.

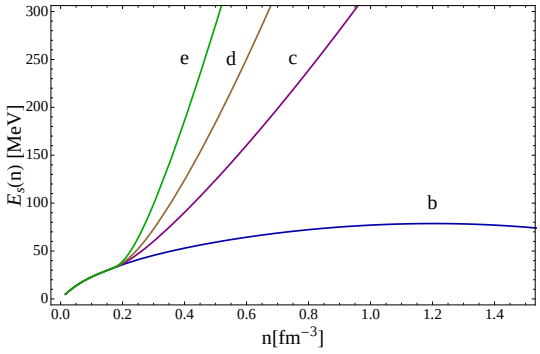

FIG. 7. Symmetry energies for the *high-*E_s models.

IV. ASTROPHYSICAL OBSERVATIONS AND SYMMETRY ENERGY CONSTRAINTS

Neutron star models must be compared with astrophysical observations to prove their validity. Although there are many astrophysical processes, not all them allow for precise information about the NS properties, like simultaneous accurate mass and radius measurements. However, recently the highest neutron star mass has been precisely measured [15] with a value around 2 $M_\odot$ placing a strong constraint to many of the existent equations of state. Even though E_s contributes to the determination of the maximum NS mass for an EOS it is the isoscalar part V that plays the major role. Therefore this measurement is not so stringent for E_s. Another pertinent result regarding NS crusts is the upper bound on the crustal moment of inertia for the Vela pulsar derived from an analysis performed by Link in [18], telling that such quantity should be higher than the 1.4% of total moment of inertia of this star. Different E_s forms will result in different crust properties to be tested against this condition. As a final constraint for the models presented here the Direct Urca cooling is considered. Low mass NS do not cool by the DUrca process according to [20]. The proton fraction of the star x should not go above the DUrca proton fraction threshold x_{DU} for those low NS masses. The DUrca threshold x_{DU} is weakly dependent density function and takes values between 0.11 and 0.15. From the β-equilibrium equations, Eq. (2), for low values of x and neglecting muons one may get the following estimation for the proton fraction in matter

$$x = \frac{1}{6 + n/n_0\ (83\ \mathrm{MeV}/E_s)^3}. \tag{14}$$

This expression implies that one natural way to fulfill this constraint is restricting E_s to low values, smaller than 80 MeV, so the resulting x always stay below x_{DU}. That is the reason we introduce the *L-high-b* models - the second sub-class in the *L-high* family, which presents soft behaviour at high density. As we will see in the following sections, this possibility has important implications for the EOS when satisfying the maximum NS mass measurement.

V. NEUTRON STAR PROPERTIES

In order to construct the neutron star profile we need to include an EOS in the whole range of densities from zero to high densities characteristic of the very central part of the star. In this study we have considered a liquid core described by EOS based on the symmetry energy forms presented in the previous section with a common isoscalar part given by the PAL parametrization. As for the crust, we have taken the SLy EOS composed of different parts whose table can be found in [16]. These two EOSs are joint at the point of equal pressure and density. This construction is not thermodynamically consistent since there is a discontinuity in chemical potentials but can be treated as an approximation that does not influence the overall macroscopic NS properties. In our approach the bottom edge of the crust is determined by the critical density $n_c(K_\mu)$ which is very close to $n_c(1 \leftrightarrow 2)$. The NS total moment of inertia and that of its crust are calculated by the following expressions, derived in the

framework of General Relativity [19], as:

$$I = \frac{J}{1 + 2GJ/R^3c^2},$$
$$\Delta I_{crust} = \frac{2}{3}(M_{crust}R^2)\frac{1 - 2GI/R^3c^2}{1 - 2GM/Rc^2} \qquad (15)$$

where $M_{crust} = M - M_{core}$ is the difference between the total mass and the mass of the core, as determined by n_c. Interestingly, the consequences of choosing $n_c(Q)$ are systematic effects of lowering the NS crust thickness and its moment of inertia. The effect was shown in [17].

A. ΔE-k models

In these models the E_s forms take finite values for very low densities in the range between $0 - 12$ MeV sharing the same high density behavior and same L value. They result into an acceptable maximum mass (of about 2 $M_\odot$) and radii between $12 - 13$ kilometers. Table I shows the transition densities for each k value: as k grows the transition density n_c lowers. A study of the behavior of the compressibility curves K_μ in this set of models show that as we increase the values of the symmetry energy at low densities, the point of vanishing K_μ occurs at lower and lower densities to finally does not appear for k greater than 14 MeV. This results into thinner and thinner neutron star crust and could be extended to crustless neutron stars, which are, however, not expected to exist according to observations. The crustal properties appear to be very sensitive to the varying portion of the symmetry energy shape, specially the crustal moment of inertia, which is shown in Fig. 8. The most likely value for the low density E_s part derived from experiment is around 10 MeV. If it is true, it will point to a very low mass of the Vela pulsar, much below 1 $M_\odot$, according to the models here. Such low masses are not favored by the supernova explosion scenarios which produce new born neutron star with masses around 1.5 $M_\odot$. This result is similar to the already reported in [2] but there it could be interpreted as an inconsistency of the model coming from the clusterization of pure neutron matter. For the models here this inconsistency has been removed but the same effect persists. Summarizing, the above results signal that the large values of E_s at $n \to 0$ are in contradiction with neutron star observations.

TABLE I. Crust-core transition densities (fm^{-3}) for the ΔE-k models.

model	$E_s(0)$	$n_c(Q)$	$n_c(K_\mu)$	$n_c(1 \leftrightarrow 2)$
ΔE-k00	0	0.0816675	0.0930797	0.0942588
ΔE-k02	2	0.0690383	0.0814262	0.0820099
ΔE-k04	4	0.053707	0.0647734	0.0647989
ΔE-k06	6	0.0399434	0.0473238	0.0474521
ΔE-k08	8	0.0306162	0.0351069	0.0353349
ΔE-k10	10	0.0248644	0.0278587	0.0288262
ΔE-k12	12	0.0209877	0.0233639	0.0257871
ΔE-k14	14	0.0173067	0.0198872	0.0215231

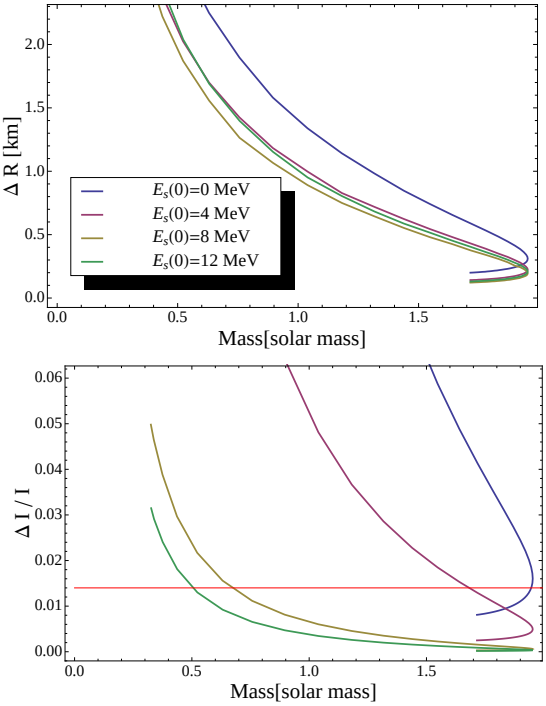

FIG. 8. Results for the ΔE-k models. *Top*: crust thickness. *Bottom*: fractional moment of inertia in the crust where the red line represent the lower bound for crustal I of the Vela pulsar. Each curve corresponds to a specific value of $k = E_s(0)$.

B. L models

A first look at the E_s form makes an impression that differences between different models in the *L-high-c* family are not large since they almost overlap and coincide at low and high density regions. Basically the only difference between them is the slope at saturation point. From table II we see that the critical density for crust-core transitions is not clearly correlated to L values: for both high and low L the critical density is large whereas for the intermediate L is lower. The behavior of the critical density with L was already analyzed in [22] and shows differences when going beyond the parabolic approximation in the nuclear energy used here. In our approach critical density differences are not very large but on the contrary the NS parameters are highly sensitive to the values of L. Both global and crustal properties of NSs are affected by such the different values of L. One may see that the star compactness $\beta \equiv GM/(Rc^2)$ is essentially changed by L specially for low NS masses. It could be naturally expected since in low mass NS central densities are relatively low and the low density E_s values

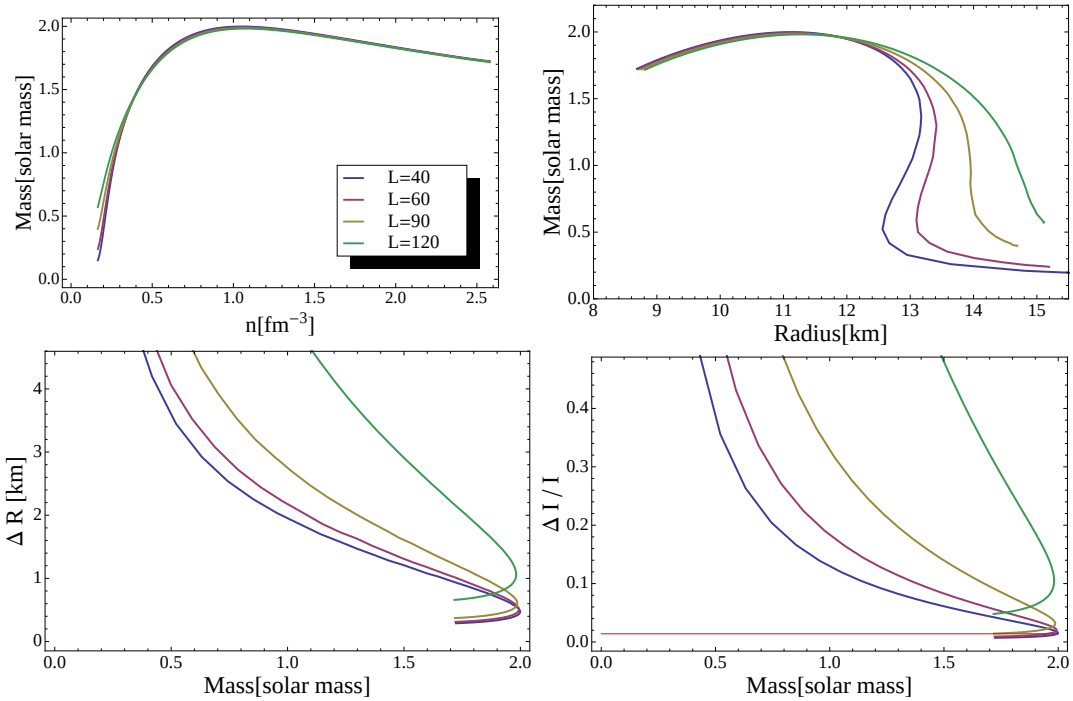

FIG. 9. Neutron star features for the *L-high-c* models.

TABLE II. Crust-core transition densities for the *L-high-c* and *L-high-b* models.

model	$n_c(Q)$	$n_c(K_\mu)$	$n_c(1 \leftrightarrow 2)$
L40-high-c	0.101234	0.107808	0.113369
L60-high-c	0.0918645	0.100315	0.103118
L90-high-c	0.0876315	0.100575	0.101674
L120-high-c	0.111214	0.139422	0.143345
L40-high-b	0.101234	0.107808	0.113369
L60-high-b	0.0918645	0.100315	0.103118
L90-high-b	0.0876315	0.100575	0.101674
L120-high-b	0.111214	0.139422	0.143345

mainly determined by L have to be relevant. The E_s slope contributes to the pressure so increasing L makes the EOS stiffer and decreases the compactness. On the contrary, a soft equation of state amplifies the effect of gravity on the star as a result of a more compact star. It is interesting that even if the crust-core transition does not behave monotonically with L, the crustal properties like thickness and moment of inertia depend clearly on the E_s slope. The larger L is, the thicker the NS crust becomes. The effect is more pronounced for the moment of inertia carried by the crust. Small values of L correspond to softer EOS resulting in a more compact star. A more compact object has stronger gravity in the crustal region, therefore the net effect is that the crust is more squeezed and contributes less to the total moment of inertia. Summarizing, in the case of L models, the crust-core transition point n_c does not play a major role in determination of the NS crustal properties but rather the gravity controlled by L is the main factor here.

C. *high-E_s* models

In this section we present results for the third family. All models in this family share the same shape of the symmetry energy up to saturation point, which means that they show the same critical density for the crust-core transition point, shown in Table III. Therefore the crustal properties are only affected by the high density shape of E_s. As one may see from Fig. 10, the compactness changes a lot for massive stars in the contrast with the previous family where this property changed for low massive stars mainly. The form of the symmetry energy at high densities changes the compactness of the NS so that the influence of gravity is different in the crust region in each model. For larger compactness the crust is more squeezed, has lower thickness and contributes less to the total moment of inertia, what is shown in Fig. 11. Those differences are more or less constant and do not depend on the total mass of a given NS. For moments

TABLE III. Crust-core transition densities for the *high-E_s* models.

model	$n_c(Q)$	$n_c(K_\mu)$	$n_c(1 \leftrightarrow 2)$
high$-E_s$ models	0.0918645	0.100315	0.103118

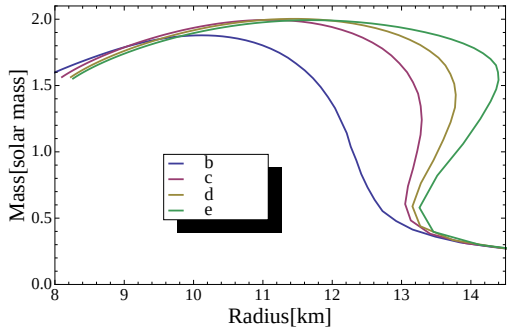

FIG. 10. Mass vs radius relation for the *high-E_s* models.

of inertia the differences are larger then for the crust thickness. Here we must emphasize that those differences comes only from the portion of E_s at very high density which is responsible for the different compactness of the star. The influence of the compactness on crustal properties of NS was estimated by an approximate formula for the moment of inertia derived in [14]:

$$\frac{\Delta I_{crust}}{I} \simeq \frac{28\pi P_t R^3}{3Mc^2}\frac{(1-1.67\beta-0.6\beta^2)}{\beta} \times\left(1+\frac{2P_t(1+5\beta-14\beta^2)}{n_t m_b c^2\beta^2}\right)^{-1} \quad (16)$$

where $P_t = p(n_t)$ and n_t (called n_c in this work) are the values of pressure and baryon number density at the crust-core transition and β is the compactness parameter. In the Fig. 11 we compare the results of this approximation and we see discrepancies that show its range of applicability. It means that the scaling of the crustal properties with the compactness is not simple and this formula must be taken with care specially in case of thick crusts.

D. Direct Urca constraint

According to [20] neutron stars with masses below 1.35 $M_\odot$ should not cool by the direct Urca process. The proton fraction of the star x should not go above the DUrca proton fraction threshold x_{DU} for those low NS masses. It is mainly determined by the symmetry energy, implying that one way to avoid violating this constraint is restricting E_s to low values so the resulting x always stay below x_{DU} (see [23] for detailed discussion). That indeed does not happen for most of the models studied in this work. The energy expression, Eq. (1), whose symmetric part is based on the PAL parametrization leads to rather soft EOS, so the central density may be easily attained by low massive stars. The critical masses satisfying the DUrca constraint are: 1.2 $M_\odot$ for ΔE-k models, 0.5 - 1.0 $M_\odot$ for *L-high-c* models and 0.5 - 1.3 $M_\odot$ for *high-E_s* models. In the particular case of the L models the higher density part of E_s is meant to be completely arbitrary and surely one can incorporate the

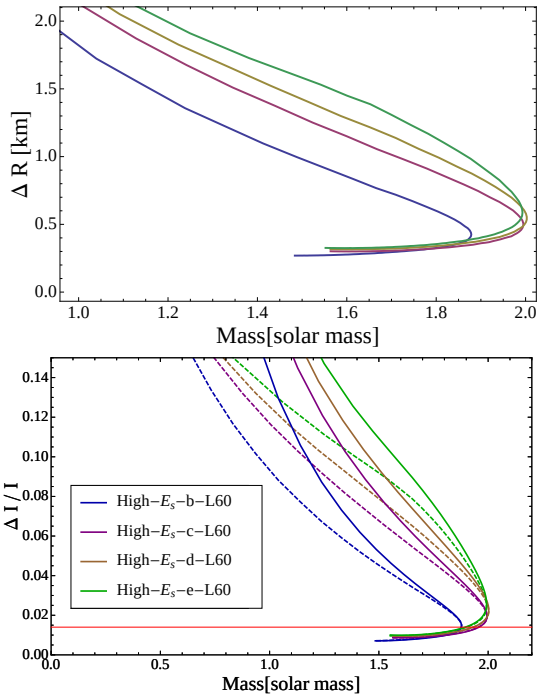

FIG. 11. Effects of the different symmetry energy forms in the *high-E_s* models for crustal thickness (top) and moment of inertia (bottom). The dashed lines correspond to the $\Delta I_{crust}/I$ derived by the approximate formula Eq. (16)

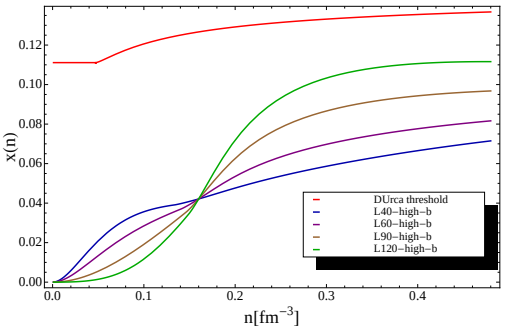

FIG. 12. The proton fraction and DUrca constraint for the *L-high-b* family.

cooling limitation easily and improve them, by means of Bézier curves. Figure 12 shows the proton fraction for the *L-high-b* models whose high density part of the symmetry energy behaves like the *b* MDI model. There it can be seen that the DUrca cooling never sets in since the proton fraction always stays below the DUrca threshold. This constraint therefore favors E_s forms which do not grow quickly with increasing density and stay bound from above. However such soft E_s leads to the maximum mass not greater than 1.85 $M_\odot$ which is in conflict with observations.

Nevertheless, there exists another possibility apart from modifications to E_s to fulfill the aforementioned re-

striction. The symmetry energy contributes to the stiffness of an EOS, but the main contribution comes from the isoscalar part of the nuclear energy. As already mentioned, in most of the models with arbitrary E_s used here the DUrca cooling sets in for unacceptable masses, due to the particular form of E_s. But if it turns out that E_s is such that x never goes above the DUrca threshold x_{DU} (like in the *L-high-b* models) then it's most likely that the isoscalar part of the PAL parametrization be wrong. It should be then properly replaced by an expression that enhances the stiffness of the EOS that would not only satisfy the DUrca constraint but at the same time contribute to the appearance of high mass neutron stars. It is worth mentioning that even if the PAL formula is highly biased, it has been useful to spot the E_s contribution to the NS physics. On the contrary, if a PAL-like isoscalar part is correct, then the symmetry energy can be very much constrained by both the cooling and the maximum mass, resulting in moderate values at low densities (to satisfy DUrca) and then increasing abruptly so high mass NS are created within the model. This result could be in fact very stringent, and its validity is to be studied and confirmed with the upcoming observations. As a final remark it is important to mention that future approaches to the EOS should take the cooling phenomenon as an important test.

VI. CONCLUSIONS

In this work we were interested in the role of the symmetry energy form played in the NS crust properties. The crust-core transition occurs well below the saturation density, so the present knowledge of the E_s parameters at this density is not sufficient to determine the transition point exactly. Moreover the symmetry energy form at higher densities, although not affecting the crust-core transition point directly is also relevant. One may say the whole shape of the E_s has to be taken into account. In order to extract the influence of different portions of the E_s shape we have constructed the three different families of symmetry energy parametrization corresponding the three range of densities: well below the saturation point, around n_0 and highly above. In each family one chosen feature was changing whereas the remaining portion of $E_s(n)$ was kept the same. This was achieved by use of Bézier curves parametrization.

In the low density regime (ΔE-k-models) the characteristic feature was the value of $E_s(n \to 0)$ being not 0 as it is suggested by some recent measurement. It appeared that high values of E_s at low density are questionable as they lead to a very thin crust, difficult to be reconciled with observations of the Vela pulsar.

In the intermediate range of density L-models the key quantity was the slope of symmetry energy L taken in the range from 40 to 120 MeV. The crust thickness and moment of inertia is very sensitive and highly increases with the value of L.

For the high densities we constructed the models preserving the same crust-core transition density but presenting completely different behaviour well above n_0, they were called *high-E_s* models. It appeared that values of E_s at high density affect the crustal properties essentially. Such effect comes from different compactness of a star. However it is difficult to find a simple scaling of crust properties with M/R, especially when the crust is thick.

The direct Urca constraint for low mass NS is related to the symmetry energy since it serves to determine the proton fraction inside the star. If the high density behavior of E_s is bounded from above to satisfy this constraint a 2 $M_\odot$ NS cannot be created by the models used here. A stiffer isoscalar part V of the nuclear energy per particle is then necessary to produce higher masses. Therefore both the heaviest observed NS and the DUrca cooling condition allow for constraining the EOS, since they are to be satisfied simultaneously. Solving this issue is surely an interesting implementation for a future work.

During the preparation of the text the authors have found the work by Lattimer et al. [24] which combines the majority of laboratory measurements. It is concluded there that the most reliable values of $S_v \approx 32$ MeV, $L \approx 50$ MeV with an error of a few MeV. This means that L-dependence on the crustal properties is almost removed. In our work, to avoid additional complexity, we have fixed the second derivative $K_s = 0$ for most presented models. Now, when the first derivative is pinned down it seems interesting to explore different K_s values, what is planned for the future.

ACKNOWLEDGMENTS

This work has been partially supported by CompStar a research networking programme of the European Science Foundation. The authors are grateful to D. Blaschke for illuminating discussions and talks on the symmetry energy subject.

Appendix: Bézier points for various models

TABLE IV. Bézier control points for the $\Delta E - k$ models. $\Delta E - k00$ is simply the PALu model.

model	$\mathbf{P}_0$	$\mathbf{P}_1$	$\mathbf{P}_2$	$\mathbf{P}_3$	$\mathbf{P}_4$
$\Delta E - k02$	(0, 2)	(0.04, 1)	(0.08, 0)	(0.12, 0)	(0.16, 0)
$\Delta E - k04$	(0, 4)	(0.04, 2)	(0.08, 0)	(0.12, 0)	(0.16, 0)
$\Delta E - k06$	(0, 6)	(0.04, 3)	(0.08, 0)	(0.12, 0)	(0.16, 0)
$\Delta E - k08$	(0, 8)	(0.04, 4)	(0.08, 0)	(0.12, 0)	(0.16, 0)
$\Delta E - k10$	(0, 10)	(0.04, 5)	(0.08, 0)	(0.12, 0)	(0.16, 0)
$\Delta E - k12$	(0, 12)	(0.04, 6)	(0.08, 0)	(0.12, 0)	(0.16, 0)
$\Delta E - k14$	(0, 14)	(0.04, 7)	(0.08, 0)	(0.12, 0)	(0.16, 0)

TABLE V. Bézier control points for the L models which are composed of two Bézier curves joint at n_0.

model	$\mathbf{P}_0$	$\mathbf{P}_1$	$\mathbf{P}_2$	$\mathbf{P}_3$	$\mathbf{P}_4$	$\mathbf{P}_5$
L40-high-c (low density)	(0, 0)	(0.0528, 22.066)	(0.106, 26.466)	(0.16, 31)		
L40-high-c (high density)	(0.16, 31)	(0.24, 37.666)	(0.32, 44.333)	(0.8, 235.372)	(1.28, 455.583)	(1.92, 819.168)
L60-high-c	(0, 0)	(0.0528, 17.6)	(0.106, 24.2)	(0.16, 31)		
	(0.16, 31)	(0.24, 41)	(0.32, 51)	(0.8, 235.372)	(1.28, 455.584)	(1.92, 819.168)
L90-high-c	(0, 0)	(0.0523, 10.9)	(0.106, 20.8)	(0.16, 31)		
	(0.16, 31)	(0.24, 469)	(0.32, 61)	(0.8, 235.372)	(1.28, 455.584)	(1.92, 819.168)
L120-high-c	(0,0)	(0.053, 4.2)	(0.106, 17.4)	(0.16, 31)		
	(0.16, 31)	(0.24, 51)	(0.32, 71)	(0.8, 235.372)	(1.28, 455.584)	(1.92, 819.168)
L40-high-b	(0, 0)	(0.0528, 22.066)	(0.106, 26.466)	(0.16, 31)		
	(0.16, 31)	(0.24, 37.666)	(0.32, 44.333)	(0.8, 72.239)	(1.28, 79.064)	(1.92, 71.955)
L60-high-b	(0, 0)	(0.0528, 17.6)	(0.106, 24.2)	(0.16, 31)		
	(0.16, 31)	(0.24, 41.000)	(0.32, 51.000)	(0.8, 72.239)	(1.28, 79.064)	(1.92, 71.955)
L90-high-b	(0, 0)	(0.0523, 10.9)	(0.106, 20.8)	(0.16, 31)		
	(0.16, 31)	(0.24, 46.000)	(0.32, 61)	(0.8,72.239)	(1.28, 79.064)	(1.92, 71.955)
L120-high-b	(0,0)	(0.053, 4.2)	(0.106, 17.4)	(0.16, 31)		
	(0.16, 31)	(0.24, 51)	(0.32, 71)	(0.8, 72.239)	(1.28, 79.064)	(1.92, 71.955)

TABLE VI. Bézier control points for the $high - E_s$ models.

model	$\mathbf{P}_0$	$\mathbf{P}_1$	$\mathbf{P}_2$	$\mathbf{P}_3$	$\mathbf{P}_4$	$\mathbf{P}_5$
low density	(0, 0)	(0.0528, 17.6)	(0.106, 24.2)	(0.16, 31)		
high density						
L60-high-b	(0.16, 31)	(0.24, 41)	(0.32, 51)	(0.8, 89.12)	(1.28, 82.86)	(1.6, 71.92)
L60-high-c	(0.16, 31)	(0.24, 41)	(0.32, 51)	(0.8, 207.26)	(1.28, 440.014)	(1.6, 626.88)
L60-high-d	(0.16, 31)	(0.24, 41)	(0.32, 51)	(0.8, 301.097)	(1.28, 813.098)	(1.6, 1146.13)
L60-high-e	(0.16, 31)	(0.24, 41)	(0.32, 51)	(0.8, 547.93)	(1.28, 1244.98)	(1.6, 1673.62)

[1] S. Kubis, Phys. Rev. C **76** (2007) 025801

[2] Kubis, S., Porebska, J.,& Alvarez-Castillo, D. E. Acta Phys.Polon.B41:2449,2010

[3] Natowitz, J. B., et al. 2010, Physical Review Letters, 104, 202501

[4] Baym, G., Bethe, H. A., & Pethick, C. J. 1971, Nuclear Physics A, 175, 225

[5] Myers, W. D., & Swiatecki, W. J. 1974, Annals of Physics, 84, 186

[6] L. -W. Chen, C. M. Ko, B. -A. Li and J. Xu, Phys. Rev. C **82**, 024321 (2010)

[7] M. B. Tsang, Y. Zhang, P. Danielewicz, M. Famiano, Z. Li, W. G. Lynch and A. W. Steiner, Phys. Rev. Lett. **102**, 122701 (2009)

[8] L. -W. Chen, C. M. Ko and B. -A. Li, Phys. Rev. Lett. **94**, 032701 (2005)

[9] M. Centelles, X. Roca-Maza, X. Vinas and M. Warda, Phys. Rev. Lett. **102**, 122502 (2009) [arXiv:0806.2886 [nucl-th]].

[10] T. Li, U. Garg, Y. Liu, R. Marks, B. K. Nayak, P. V. M. Rao, M. Fujiwara and H. Hashimoto *et al.*, Phys. Rev. Lett. **99**, 162503 (2007) [arXiv:0709.0567 [nucl-ex]].

[11] S. Kowalski, J. B. Natowitz, S. Shlomo, R. Wada, K. Hagel, J. Wang, T. Materna and Z. Chen *et al.*, Phys. Rev. C **75**, 014601 (2007) [nucl-ex/0602023].

[12] http://en.wikipedia.org/wiki/Bezier_curve
Farin, Gerald, Curves and surfaces for computer-aided geometric design (4 ed.), Elsevier Science & Technology Books, 1997

[13] Prakash, M., Lattimer, J. M., & Ainsworth, T. L. 1988, Physical Review Letters, 61, 2518

[14] Lattimer, J. M., & Prakash, M. 2001, Astrophys. J., 550, 426

[15] P. B. Demorest, T. Pennucci, S. M. Ransom, M. S. E. Roberts and J. W. T. Hessels, *Nature*, **467**, 1081 (2010).

[16] http://www.ioffe.ru/astro/NSG/NSEOS/

[17] D.E. Alvarez-Castillo, PhD Thesis, 2012.X

[18] B. Link, R. I. Epstein and J. M. Lattimer, Phys. Rev. Lett. **83** (1999) 3362

[19] Ravenhall, D. G., & Pethick, C. J. 1994, Astrophys. J.,

424, 846
[20] Popov, S., Grigorian, H., Turolla, R., & Blaschke, D. 2006, A&A, 448, 327
[21] L. -W. Chen, C. M. Ko and B. -A. Li, Phys. Rev. C **76**, 054316 (2007)
[22] Xu, J., Chen, L.-W., Li, B.-A., & Ma, H.-R. 2009, Phys. Rev. C, 79, 035802
[23] J. M. Lattimer, M. Prakash, C. J. Pethick and P. Haensel, Phys. Rev. Lett. **66**, 2701 (1991).
[24] Lattimer, J. M., & Lim, Y. 2012, arXiv:1203.4286